Journal of Hazardous Materials 353 (2018) 312–319

Contents lists available at ScienceDirect

Journal of Hazardous Materials

journal homepage: www.elsevier.com/locate/jhazmat

Removal of arsenic and mercury species from water by covalent triazine framework encapsulated γ-Fe_2O_3 nanoparticles

Karen Leus[a,1,*], Karel Folens[b,1], Nina Ricci Nicomel[b], Jeffrey Paulo H. Perez[a,b,2], Maria Filippousi[c], Maria Meledina[c], Marinela M. Dîrtu[d], Stuart Turner[c], Gustaaf Van Tendeloo[c], Yann Garcia[d], Gijs Du Laing[b], Pascal Van Der Voort[a,*]

[a] Department of Chemistry, Center for Ordered Materials, Organometallics and Catalysis (COMOC), Faculty of Sciences, Ghent University, Krijgslaan 281 (S3), 900 Ghent, Belgium
[b] Laboratory of Analytical Chemistry and Applied Ecochemistry, Faculty of Bioscience Engineering, Ghent University, Coupure Links 653, 9000 Ghent, Belgium
[c] EMAT, University of Antwerp, Groenenborgerlaan 171, 2020 Antwerpen, Belgium
[d] Institute of Condensed Matter and Nanosciences, Molecules, Solids, Reactivity (IMCN/MOST) Université Catholique de Louvain, Place Louis Pasteur 1, 1348 Louvain-la-Neuve, Belgium

GRAPHICAL ABSTRACT

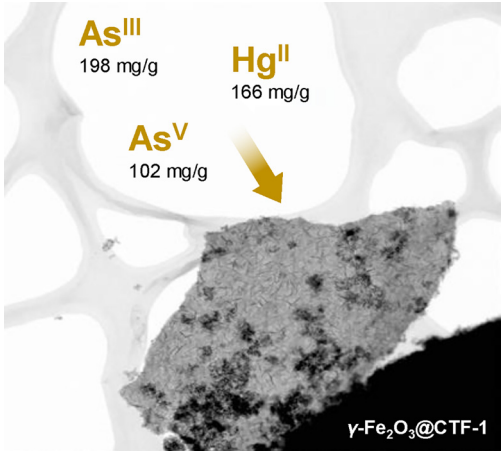

ARTICLE INFO

Keywords:
Arsenic
Mercury
Covalent organic frameworks
Iron oxide nanoparticles
Water treatment

ABSTRACT

The covalent triazine framework, CTF-1, served as host material for the *in situ* synthesis of Fe_2O_3 nanoparticles. The composite material consisted of 20 ± 2 m% iron, mainly in γ-Fe_2O_3 phase. The resulting γ-Fe_2O_3@CTF-1 was examined for the adsorption of As^{III}, As^{V} and Hg^{II} from synthetic solutions and real surface-, ground- and wastewater. The material shows excellent removal efficiencies, independent from the presence of Ca^{2+}, Mg^{2+} or natural organic matter and only limited dependency on the presence of phosphate ions. Its adsorption capacity towards arsenite (198.0 mg g^{-1}), arsenate (102.3 mg g^{-1}) and divalent mercury (165.8 mg g^{-1}) belongs amongst the best-known adsorbents, including many other iron-based materials. Regeneration of the adsorbent can be achieved for use over multiple cycles without a decrease in performance by elution at 70 °C with 0.1 M

* Corresponding authors.
E-mail addresses: Karen.Leus@UGent.be (K. Leus), Pascal.Vandervoort@UGent.be (P. Van Der Voort).
[1] Both authors contributed equally to this work.
[2] Present address: Helmholtz Centre Potsdam - GFZ German Research Centre for Geosciences, Telegrafenberg, 14473 Potsdam, Germany.

https://doi.org/10.1016/j.jhazmat.2018.04.027
Received 12 December 2017; Received in revised form 12 April 2018; Accepted 13 April 2018
Available online 16 April 2018
0304-3894/

NaOH, followed by a stirring step in a 5 m% H_2O_2 solution for As or 0.1 M thiourea and 0.001 M HCl for Hg. In highly contaminated water (100 µg L^{-1}), the adsorbent polishes the water quality to well below the current WHO limits.

1. Introduction

Heavy metals and metalloids pose a widespread issue as they are persistent in the environment. Arsenic and mercury are highly toxic to all life forms. Remediation is challenging, in particular to achieve the very low standard in drinking water of 10 µg L^{-1} As [1] and 1 µg L^{-1} Hg [2]. Moreover, the elemental speciation complicates the treatment process since different forms of arsenic and mercury can exist simultaneously. Remediation requires a technique that is capable of removing all forms [3]. In aqueous media, arsenite (As^{III}), arsenate (As^{V}) and divalent mercury (Hg^{II}) are the most common oxidation states. Among the available technologies for removal of inorganic arsenic and mercury from solution, adsorption is the most widely studied method [4].

Within this context, several metal-based engineered nanoparticles have been examined, especially Fe_xO_y based nanoparticles (NPs) [5,6]. The oxidation state of iron is determinative in the removal mechanism, as it can contribute to oxidation/reduction reactions next to adsorption [7]. Although Fe_xO_y NPs demonstrated to be efficient and fast in arsenite and arsenate removal [8], the stability in water is rather limited due to oxidation and agglomeration processes, which will induce a decrease in the available surface area and therefore result in a reduced capacity and selectivity [9].

A way to circumvent this stability issue is to encapsulate these NPs into water-stable porous materials. A novel class of materials, covalent organic frameworks (COFs), is very promising for such application. COFs are porous aromatic polymers with pure organic groups connected *via* robust covalent bonds. Since their existence, a variety of COFs have been constructed by utilizing different linkages such as boronate, imine, hydrazone and triazine moieties [10]. The latter moiety is formed by a trimerization reaction of aromatic nitriles to triazine rings giving rise to the so called covalent triazine frameworks (CTFs). CTFs have been synthesized for the first time by Thomas and coworkers in 2008 by using an ionothermal synthesis route in which $ZnCl_2$ acts as solvent and as catalyst [11]. Due to their promising features *e.g.* large surface area, high porosity, low density, facile synthesis and relatively cheap monomeric linkers, CTFs have been examined already in a wide range of interesting applications including gas adsorption or storage, supercapacitors and in catalysis [12–14]. A few pioneering studies appeared on environmental applications focusing mainly on the adsorption of organic dyes and aromatic compounds [15–19].

In this study, the embedding of γ-Fe_2O_3 engineered nanoparticles in the CTF-1 material is presented. A thorough characterization of the material is realized by several (spectroscopic) methods, before evaluating it as novel adsorbent towards remediation of inorganic contaminants in water. Special attention is given to the kinetics, presence of other compounds, use of domestic wastewater and regeneration of the adsorbent, since the latter can successfully extend the adsorbent lifetime and hence suppress the associated costs of water purification.

2. Materials and methods

2.1. Material synthesis

The synthesis of CTF-1 was based on the procedure reported by Thomas et al. [11]. Under an inert atmosphere, 10 g $ZnCl_2$ and 2 g 1,4-dicyanobenzene were mixed in an pyrex ampoule, sealed and heated to 400 °C for 4 h and kept at this temperature for 40 h. In order to remove $ZnCl_2$, the obtained black powder was stirred subsequently in water and 1 M HCl at room temperature for 24 h. Afterwards, the black powder was filtered and dried under vacuum at 120 °C prior to analysis. The Fe_2O_3 nanoparticles were synthesized *in situ* by adding 406.9 mg of $FeCl_3 \cdot 6\ H_2O$ and 152.6 mg of $FeCl_2 \cdot 4\ H_2O$ into a 100 mL aqueous suspension containing 0.5 g CTF-1. The resulting mixture was stirred for 2 h under an inert atmosphere, followed by the addition of 15 mL NH_3 solution. After stirring for 10 min, the γ-Fe_2O_3@CTF-1 material was filtered and washed thoroughly with water and acetone. Hereafter, the material was dried under vacuum at 90 °C for 12 h.

2.2. Material characterization

Nitrogen sorption isotherms were measured on a Belsorp-mini II apparatus at 77 K. The samples were activated under vacuum overnight at 120 °C prior to surface area analysis to remove adsorbed water. Elemental analysis of the material's Fe content was determined in triplicate ($N = 3$) by Inductively Coupled Plasma – Optical Emission Spectroscopy (Varian MPX, Palo Alto, CA) at λ 238.204 nm. The As and Hg concentrations were determined by Inductively Coupled Plasma – Mass Spectrometry (Elan DRCe II, Perkin Elmer SCIEX, Waltham, MA) at m/z 91 (AsO^+) and m/z 202, respectively. As reacted with O_2 gas that was added at a flow rate of 0.4 mL min^{-1} to the reaction cell.

A combination of angular dark field scanning electron microscopy (ADF-STEM) imaging with energy-dispersive X-ray spectroscopy (EDX) spectroscopy, electron energy loss spectroscopy (EELS) and ^{57}Fe Mössbauer spectroscopy was used to provide the information on the resulting morphology and to determine the valency of iron in the iron oxide nanoparticles. Transmission electron microscopy (TEM) micrographs, HAADF-STEM images and EDX spectra were recorded using a FEI Tecnai Osiris electron microscope operated at 200 kV, equipped with a ChemiSTEM system. STEM-EELS experiments were carried out on a Titan "cubed" microscope, equipped with an aberration corrector, a monochromator and a high-resolution GIF QUANTUM energy filter. For STEM-EELS experiments, the microscope was operated at 120 kV. The electron monochromator was excited to provide an estimated EELS energy resolution of 150 meV. The convergence angle used in the STEM-EELS experiments was 18 mrad, while the acceptance angles for EELS analyses were 160 and 85 mrad, respectively. ^{57}Fe Mössbauer spectra were recorded in transmission geometry with a conventional Mössbauer spectrometer equipped with a ^{57}Co(Rh) radioactive source operating at room temperature. The samples were sealed in aluminum foil and mounted on a nitrogen Oxford bath cryostat. The spectra were fitted to the sum of Lorentzians by a least-squares refinement using or Recoil 1.05 Mössbauer Analysis Software [20]. All isomer shifts refer to α-Fe at room temperature.

2.3. Adsorption experiments

A quantity of 40 mg γ-Fe_2O_3@CTF-1 is brought in contact for 24 h at room temperature with 10 mL of 10.0 mg L^{-1} As^{III}, As^{V} and Hg^{II} solution using the respective metal salts $NaAsO_2$, $Na_2HAsO_4 \cdot 7H_2O$ and $Hg(NO_3)_2$. Phase separation is done by centrifugation at 9000 rpm and subsequent filtration using a membrane filter of 0.45 µm pore size. Finally, the As and Hg concentrations in the filtrate are measured by ICP-MS. The kinetics are studied and fitted to the pseudo-second order model according Eq. (1).

$$\frac{t}{q_t} = \frac{t}{q_e} + \frac{1}{k_2 q_e^2} \quad (1)$$

Desorption experiments were carried out in triplicate ($N = 3$) with

0.1 M NaOH solution for As and 0.1 M thiourea with 0.001 M HCl for Hg, at 70 °C for 30 min per run ($N = 8$), followed by identical phase separation and monitoring of As and Fe concentrations. After desorption of As, the material is stirred for an additional 2 h at room temperature in a 5 m% H_2O_2 solution and regularly opened for release of pressure generated by O_2 gas. Microfiltration of the product, whereby the filtrate was analysed for Fe leaching, proceeded and the solid was dried under vacuum overnight at 90 °C.

3. Results and discussion

3.1. Material characterization

The obtained Fe_2O_3@CTF-1 material has a pore volume of 0.46 $cm^3 g^{-1}$. The Langmuir surface area after introduction of 20 ± 2 m% Fe in form of engineered nanoparticles is 1049 m^2 g^{-1}, which is about 10% lower than the pristine CTF-1, as is seen in Fig. 1. After the introduction of the nanoparticles, some additional intraparticle porosity can be observed in the high pressure regime of the isotherm.

In Fig. 2, γ-Fe_2O_3@CTF-1 is visualized by means of electron microscopy. High resolution transmission electron microscopy (HR-TEM) depicts the CTF-1 structure (Fig. 2a). Bright contrast features decorating the bigger CTF-1 particles after the loading procedure correspond to the iron oxide nanoparticles. The ADF-STEM image, shown in Fig. 2b confirms that the nanoparticles (*ca.* 5–7 nm) are distributed throughout the CTF-1. EDX elemental map of Fe of γ-Fe_2O_3@CTF-1 (Fig. 2c) reveal the equal distribution of Fe throughout the CTF particles. No significant surface enrichment is observed.

EELS is known to be a direct technique for "fingerprinting" the oxidation state and coordination of transition metals and was exploited to identify the phase of the iron oxide nanoparticles. Fig. 3 contains EEL spectra of the Fe_2O_3@CTF-1. Looking at the recorded EEL spectrum, one can clearly observe a small pre-peak in the Fe L_3-edge, and a post-peak in the Fe L_2-edge (Fig. 3b). These features in the Fe 2p L-edge are indicative of γ-Fe_2O_3 [21]. Moreover, the iron sites in the material were quantitatively evaluated from the corresponding ^{57}Fe Mössbauer lines presented in Table S1. The iron phase has 88 % of Fe^{III} species present within the γ-Fe_2O_3@CTF-1 form which are preserved during the multiple cycles of adsorption and desorption (see Fig. 4).

3.2. Dependence of adsorption on pH

The influence of the pH on arsenic removal by our novel adsorbent was investigated since this is known to have a significant impact on the removal of arsenic from water [17]. In Fig. 5, the uptake of As^{III}, As^{V} and Hg^{II} by γ-Fe_2O_3@CTF-1 is presented at different pH values. The optimal removal of all species is observed in the neutral pH domain, which is the pH level that corresponds very well to natural waters. The removal of Hg decreases only at the pH of 11, presumably due to the formation of stable hydroxide complexes, withdrawing free ions from solution. Overall, the embedding of γ-Fe_2O_3 nanoparticles allows for high removal efficiencies under environmentally relevant conditions.

3.3. Adsorption uptake and isotherms

The maximum adsorption capacities of γ-Fe_2O_3@CTF-1 for As^{III}, As^{V} and Hg^{II} were assessed using the Langmuir isotherms presented in Fig. S1 and Table S2. These values are shown in Tables 1 and 2 in comparison to those of pure iron oxide nanoparticles, other Fe-based adsorbents supported on (carbon-based) porous frameworks and surface-modified iron oxide nanoparticles. Most of the adsorbents were tested at near-neutral pH values, which can be a good basis for comparison, considering that the solution pH is an important parameter affecting the adsorption process.

Adsorption of As^{III} and As^{V} has already been studied on different iron oxides nanoparticles [44]. In the work done by Lin et al. [22], magnetic γ-Fe_2O_3 nanoparticles achieved maximum adsorption capacities of 67.0 mg g^{-1} and 95.4 mg g^{-1} for As^{III} and As^{V}, respectively (Table 1 entry 1). These values are relatively high compared to other Fe-based adsorbents reported in literature. However, the adsorption capacity of this material is limited by the occurrence of some agglomeration, which is also the reason why its regeneration process is inhibited [22]. In a similar study performed by Kilianová et al. [23], ultrafine superparamagnetic γ-Fe_2O_3 nanoparticles were also used to remove arsenic from water (Table 1 entry 2). In this study, the adsorbent was only examined for arsenate, which is a drawback taking into account that arsenite is more harmful than arsenate as the former is more cytotoxic, genotoxic, mobile, and soluble [45]. The same is true for the work done by Faria et al. [24], in which δ-FeOOH nanoparticles were used (Table 1 entry 3).

The maximum adsorption capacities of some Fe-based adsorbents supported by a carbon-based framework were also included in Table 1. In the work of Reed et al. [26], Fe^{III} impregnated activated carbon was investigated for As^{III} and As^{V} removal. This adsorbent showed q values of 4.67 and 4.50 mg g^{-1} for As^{III} and As^{V}, respectively (Table 1 entry 5), whereas in the study of Zhang et al. [27], a magnetite-impregnated activated carbon fiber (MACF) was synthesized (Table 1 entry 6) exhibiting a similar uptake for As^{V}. Magnetite nanoparticles were also supported on multiwalled carbon nanotubes (Table 1 entry 10) demonstrating a simultaneous removal of As^{III} and As^{V} from aqueous solutions with a capacity of 53.2 and 39.1 mg g^{-1}, respectively [31].

Besides the evaluation of Fe_xO_y-based adsorbents, zero-valent iron (nZVI) adsorbents were also examined. For instance, in the work of Zhu et al. [29], nZVI was supported onto activated carbon (Table 1 entry 8). Relatively fast kinetics for the removal of arsenic was observed, however, both arsenite and arsenate removal were largely affected by the presence of anions and humic acid, with silicate and phosphate showing the most significant effect. In contrast to this work, Wang et al. [34] obtained a more effective adsorbent operating at a lower dose by using reduced graphite oxide (RGO) as support to anchor the nZVI (Table 1 entry 13). In comparison to these previous studies, much higher adsorption capacities were obtained for As^{III} and As^{V} by using Fe_2O_3@CTF-1 as adsorbent. At pH 7, adsorption capacities of 198 and 102.3 mg g^{-1} were obtained for As^{III} and As^{V}, respectively (Table 1 entry 16). These values are significantly higher than the pristine CTF-1 material having a maximum adsorption capacity for As^{V} of only 28.60 mg g^{-1} (Table 1 entry 15). These results are in correspondence to the work of Shang et al. [46] in which also higher adsorption capacities for As^{III} then for As^{V} were observed. The authors addressed this observation to the difference in surface charge of As^{III} and As^{V} below pH 9.2.

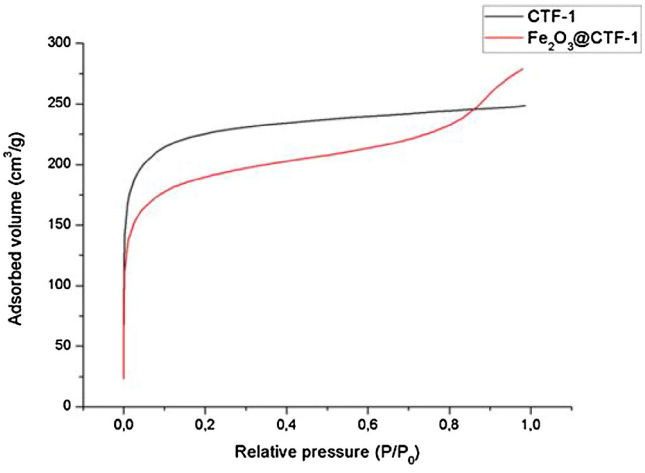

Fig. 1. N_2 adsorption isotherms of CTF-1 and γ-Fe_2O_3@CTF-1.

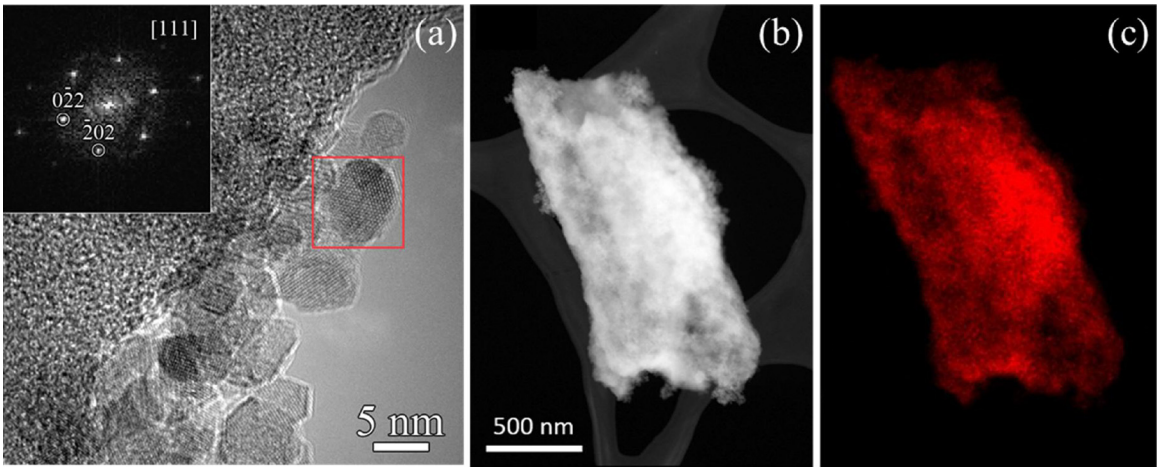

Fig. 2. Visualisation of γ-Fe_2O_3@CTF-1 by (a) HR-TEM (Inset: FFT pattern along the [111] zone axis, taken from the area marked with red revealing the γ-Fe_2O_3 phase of iron oxide nanoparticles (JCPDS 39–1346)), (b) ADF-STEM image and (c) EDX elemental map, revealing the presence of Fe (red) in the material (For interpretation of the references to colour in this figure legend, the reader is referred to the web version of this article).

Iron oxide nanoparticles have also shown good performance for the adsorption of mercury. Etale et al. [36] tested γ-Fe_2O_3 nanoparticles and achieved a maximum adsorption capacity of 8.9 mg g^{-1} for Hg^{II} (Table 2 entry 1). This value is similar to the maximum adsorption study obtained for Fe_3O_4 nanoparticles (Table 2 entry 2) [37]. However, pristine iron oxide nanoparticles are chemically unstable under ambient conditions, usually easily oxidized in air or easily dissolved in acidic medium [47,48]. In addition, they also exhibit low affinity for mercury species.

In order to increase their stability and affinity for mercury, surface modification is usually employed on iron oxide nanoparticles using polymers and functionalized chemical coatings. Liu and co-workers [38] coated Fe_3O_4 NPs with humic acid (HA) in order to reduce aggregation, and improve its affinity for mercury due to the carboxylic, phenolic and quinone functional moieties attached to it (Table 2 entry 3). The maximum metal uptake was found to be 97.7 mg Hg^{II} g^{-1} adsorbent, which is five times higher than the pristine Fe_3O_4. Aside from HA, another commonly used surface coating for iron NPs is silica. It acts both as a stabilizer and an inorganic shell wherein specific functionalities can be grafted through silanization. Zhang et al. [37] utilized 3-mercaptopropyltrimethoxysilane (MPTS) as the thiol precursor for the silanization reaction at the surface of silica-coated Fe_3O_4 (Table 2 entry 4). Fe_3O_4@SiO_2-SH has a maximum adsorption capacity of 148.8 mg g^{-1}, which is significantly higher compared to that of pristine and silica-coated Fe_3O_4 nanoparticles.

Porous framework-supported iron oxide nanoparticles have also been examined for the removal of mercury. Huang et al. [42] designed a thiol-functionalized core-shell magnetic metal organic framework (MOF) composite, Fe_3O_4@SiO_2@HKUST-1 which was evaluated for Hg^{2+} adsorption, resulting in a maximum adsorption capacity of 264 mg g^{-1} (Table 2 entry 8). Despite its excellent performance in Hg removal, it was chemically unstable and transformed after exposure to acidic condition for less than 30 min. Furthermore, significant leaching of Cu^{2+} was also observed from the MOF composite, which is not favorable for water treatment as it releases a secondary pollutant. The same group also prepared a thiol-functionalized Fe_3O_4@SiO_2/UiO-66, which is more chemically stable and has a maximum adsorption capacity of 282 mg g^{-1} (Table 2 entry 9) [43].

In addition to its excellent adsorption capacity, γ-Fe_2O_3@CTF-1 can also remove arsenic and mercury species at low contaminant concentration range (Table 3). At an initial element concentration of 100 µg L^{-1}, the equilibrium concentrations after adsorption onto γ-Fe_2O_3@CTF-1 were able to meet the stringent standard limits for As and Hg in drinking water of 10 µg L^{-1} and 1 µg L^{-1}, respectively.

3.4. Influence of competing ions

The presence of other compounds, such as calcium, magnesium, phosphate or natural organic matter (NOM), can affect the removal behavior due to competition for the binding sites at the adsorbent [49]. The effects were evaluated by separately spiking excess amounts of Ca^{2+}, Mg^{2+} and PO_4^{3-} ions and NOM to solutions of arsenite and arsenate. Moreover, the arsenic and mercury removal was evaluated in real water bodies of surface-, ground- and domestic wastewater of which the chemical composition is given in Table 4. Fig. 6 illustrates that no significant decrease in the efficiency of γ-Fe_2O_3@CTF-1 towards

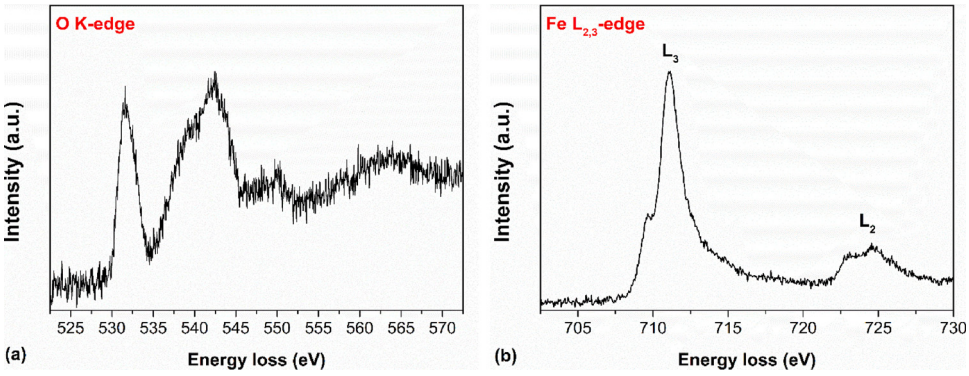

Fig. 3. EEL spectra of the γ-Fe_2O_3@CTF-1 showing (a) O K- and (b) Fe $L_{2,3}$-edges.

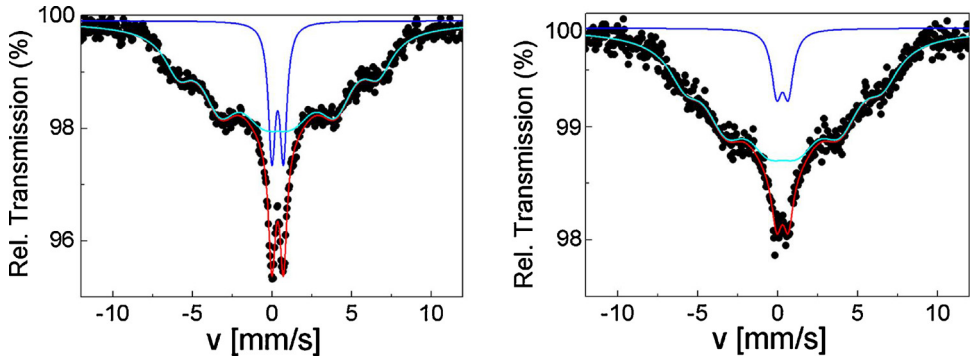

Fig. 4. Mössbauer spectra of the pristine Fe_2O_3@CTF-1 (left) and after washing with 5 m% H_2O_2 solution after As desorption (right).

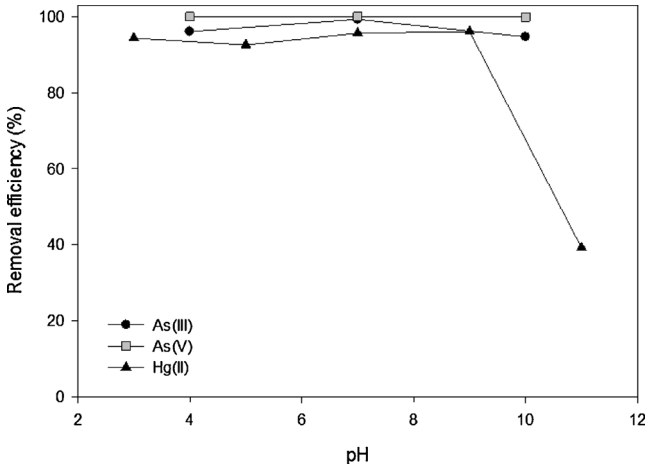

Fig. 5. Dependence of the removal efficiency on the solution pH for removal of arsenic (100 µg L^{-1}) and mercury (10 µg L^{-1}) species by γ-Fe_2O_3@CTF-1.

Table 1
Adsorption capacities and experimental conditions of different iron-impregnated carbon-based adsorbents towards arsenic species in water at room temperature.

Entry	Adsorbent	pH	Contact time (h)	Adsorption capacity (mg g^{-1})		Reference
				As^{III}	As^{V}	
1	Magnetic γ-Fe_2O_3 nanoparticles	6 (As^{III})^{V})	*	67.0	95.4	[22]
2	γ -Fe_2O_3 nanoparticles	7	*	*	45.0	[23]
3	δ-FeOOH nanoparticles	7	24	*	37.3	[24]
4	GAC-Fe	7	72	0.0231	0.0248	[25]
5	Fe_xO_yAC	7	48	4.67	4.50	[26]
6	MACF	4	24	*	4.16	[27]
7	FeAC	6	24	38.8	51.3	[28]
8	nZVI/AC	6.5	72	18.2	12.0	[29]
9	Coconut-shell carbon pretreated with Fe(III)	5	24	*	4.53	[30]
10	Fe_3O_4-MWNTs	*	*	53.2	39.1	[31]
11	e-MWCNT/Fe^{2+}	4	*	*	23.47	[32]
12	RH-FeOOH	4	6	*	2.50	[33]
13	nZVI–RGO	7	4	35.8	29.0	[34]
14	Fe-impregnated biochar	5.8	*	*	2.16	[35]
15	CTF-1	8	24	*	28.6	This study
16	γ-Fe_2O_3@CTF-1	7	24	198.0	102.3	This study

Table 2
Adsorption capacities and experimental conditions of different modified and encapsulated iron oxide adsorbents towards mercury species in water at room temperature.

Entry	Adsorbent	pH	Contact time (h)	Adsorption capacity (mg g^{-1})	Reference
1	γ-Fe_2O_3 nanoparticles	3	0.5	8.9	[36]
2	Fe_3O_4 nanoparticles	6.5	4	20.0	[37]
3	Humic acid-coated Fe_3O_4	6.0	0.5	97.7	[38]
4	Fe_3O_4@SiO_2-SH	6.5	4	148.8	[37]
5	MPTS-mesoporous Fe_3O_4/C@SiO_2	6.5	8	118.6	[39]
6	GO-Fe_3O_4	5.0	3	16.6	[40]
7	Fe_3O_4-rGO	7.0	3	118.6	[41]
8	Bi-I-functionalized Fe_3O_4@SiO_2@HKUST-1	3.0	0.33	264	[42]
9	SH-Fe_3O_4@SiO_2/UiO-66	3.0	1	282	[43]
10	CTF-1	3-5	24	32.8	This study
11	γ-Fe_2O_3@CTF-1	3-5	24	165.8	This study

Table 3
Equilibrium concentration and removal efficiency after adsorption of 100 µg L^{-1} onto γ-Fe_2O_3@CTF-1.

Species	C_e (µg L^{-1})	Drinking water standard (µg L^{-1})	Removal efficiency (%)
AsIII	3.3	10	97.1
As(V)	3.7	10	96.6
Hg(II)	1.0	1	99.0

Table 4
Chemical composition of surface-, ground- and domestic wastewater used to evaluate the adsorption of As^{III}, As^{V} and Hg^{II} on γ-Fe_2O_3@CTF-1.

Parameter	Unit	Surface water	Groundwater	Domestic wastewater
pH		7.9	8.0	7.4
$EC_{25\,°C}$	µS cm^{-1}	142	939	1094
TOC	mg L^{-1}	NA	8.5	11.2
Ca^{2+}	mg L^{-1}	1.1	78.0	
Mg^{2+}	mg L^{-1}	0.1	10.4	
Cl^-	mg L^{-1}	1.4	63.1	
NO_2^-	mg L^{-1}	1.1	0.5	
NO_3^-	mg L^{-1}	5.3	22.1	
PO_4^{3-}	mg L^{-1}	1.0	< 2.0	
SO_4^{2-}	mg L^{-1}	3.4	77.0	

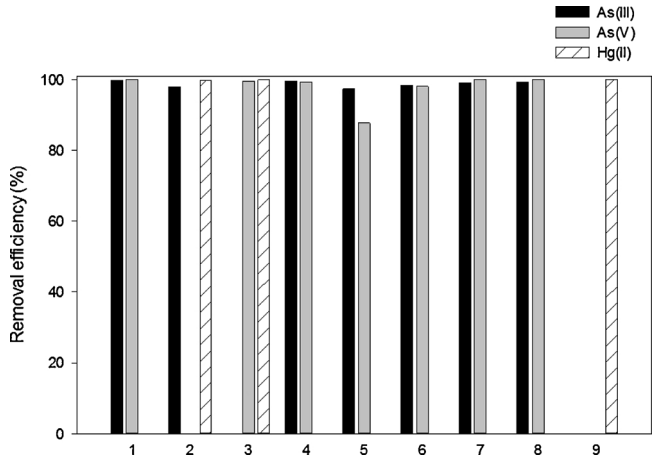

Fig. 6. Removal efficiency (%) of γ-Fe_2O_3@CTF-1 for As^{III} (black), As^{V} (grey) and Hg^{II} (white dashed) in the presence of potentially interfering compounds: (1) control, (2) As^{III} and Hg^{II} together (10 mg L^{-1} of each component), (3) As^{V} and Hg^{II} together (10 mg L^{-1} of each component), (4) 25 mg L^{-1} Ca^{2+} and 25 mg L^{-1} Mg^{2+}, (5) 25 mg L^{-1} phosphate, (6) 25 mg L^{-1} NOM, (7) surface water, (8) groundwater and (9) domestic wastewater.

arsenic and mercury species was observed under the described conditions. Even if both species (As^{III}/As^{V} and Hg^{II}) were present no loss in the removal efficiency was noted demonstrating the potential use of this CTF material as multifunctional adsorbent. The presence of NOM or Ca^{2+} can contribute to the binding of inorganic contaminants by, respectively, a direct binding to amine functional groups on NOM or through cation bridges [50]. Only negatively charged phosphate ions reduce the removal efficiency of As^{V} by 12.3 % due to the similar tetrahedral chemical structure they possess.

The kinetics of the adsorption process was studied for the inorganic contaminants. The resulting data were plotted according to the pseudo-second order kinetic model. Fig. 7 and Table 5 clearly show that the kinetics of As and Hg adsorption are obviously very fast, reaching equilibrium already after a few minutes.

3.5. Desorption and adsorbent regeneration

To study the regeneration potential of γ-Fe_2O_3@CTF-1, desorption experiments were performed. Full desorption of As and reactivation of the adsorbent was established by washing it with 0.1 M NaOH at 70 °C and 5 m% H_2O_2 solution. The loaded Hg could be desorbed by washing with a solution of 0.1 M thiourea in 0.001% HCl, having a pH of 3.2,

Table 5
Parameters of the pseudo-second order equation model describing the kinetics of As^{III}, As^{V} and Hg^{II} adsorption on γ-Fe_2O_3@CTF-1.

Model	Constant	As^{III}	As^{V}	Hg^{II}
Pseudo-second order	Q (mg g^{-1})	2.554	1.859	2.54
	$1/k_2$ (mg min g^{-1})	−2.688	−3.709	0.013
	R^2	0.99994	0.99994	0.9999

also at 70 °C. Fig. 8 shows that a same removal performance for As^{III} and Hg^{II} can be achieved in additional cycles. For As^{V}, a slightly decreased performance is observed in the third and fourth cycle of adsorption. This decrease might be attributed to the mobility of the Fe_2O_3 nanoparticles, which tend to migrate to the surface of the material to form Fe_2O_3 aggregates. The latter hypothesis was supported by EDX-STEM images obtained after the adsorption of 5 m% As^{V}, showing the formation of Fe_2O_3 aggregates at the surface (see Fig. S2). The cumulative leaching of Fe from the adsorbent was minimized to < 0.2% after 4 cycles.

4. Conclusions

The use of Fe_2O_3 nanoparticles encapsulated in the CTF-1 was presented as first for the abatement of two major inorganic pollutants in aqueous media. Characterization by Mössbauer spectroscopy and EELS revealed the γ-Fe_2O_3 phase of iron oxide nanoparticles. The corresponding paramagnetic properties of maghemite can be exploited during phase separation. The adsorption capacity of γ-Fe_2O_3@CTF-1 reached 198.0 mg g^{-1} for As^{III}, 102.3 mg g^{-1} for As^{V} and 165.8 mg g^{-1} for Hg^{II}, which is higher in comparison to the pristine CTF-1 and other state-of-the-art adsorbents, including other iron-based materials. The presence of potentially interfering compounds, such as Ca^{2+}, Mg^{2+} and NOM, did not affected the adsorption performance of As. In natural water bodies, high removal efficiencies were maintained for As and Hg, demonstrating its applicability in real-life situations. Moreover, the material could be reused over multiple cycles while maintaining good adsorption performance.

Acknowledgments

Karen Leus acknowledges financial support from Ghent University. Nina Ricci Nicomel and Jeffrey Paulo H. Perez thank the funding of the VLIR-UOS. Marinela M. Dîrtu acknowledges F.R.S.-FNRS for a Chargé de recherches position. Stuart Turner gratefully acknowledges the FWO Vlaanderen for a post-doctoral scholarship. The Titan microscope used

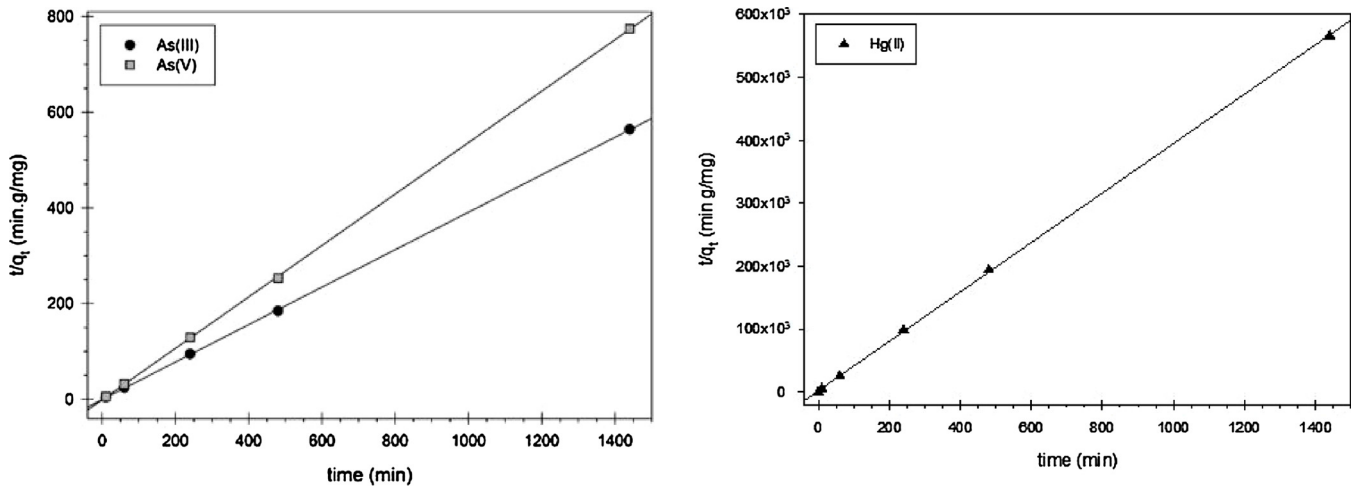

Fig. 7. Kinetics of As^{III}, As^{V} (left) and Hg^{II} (right) adsorption on γ-Fe_2O_3@CTF-1 according the pseudo-second order model.

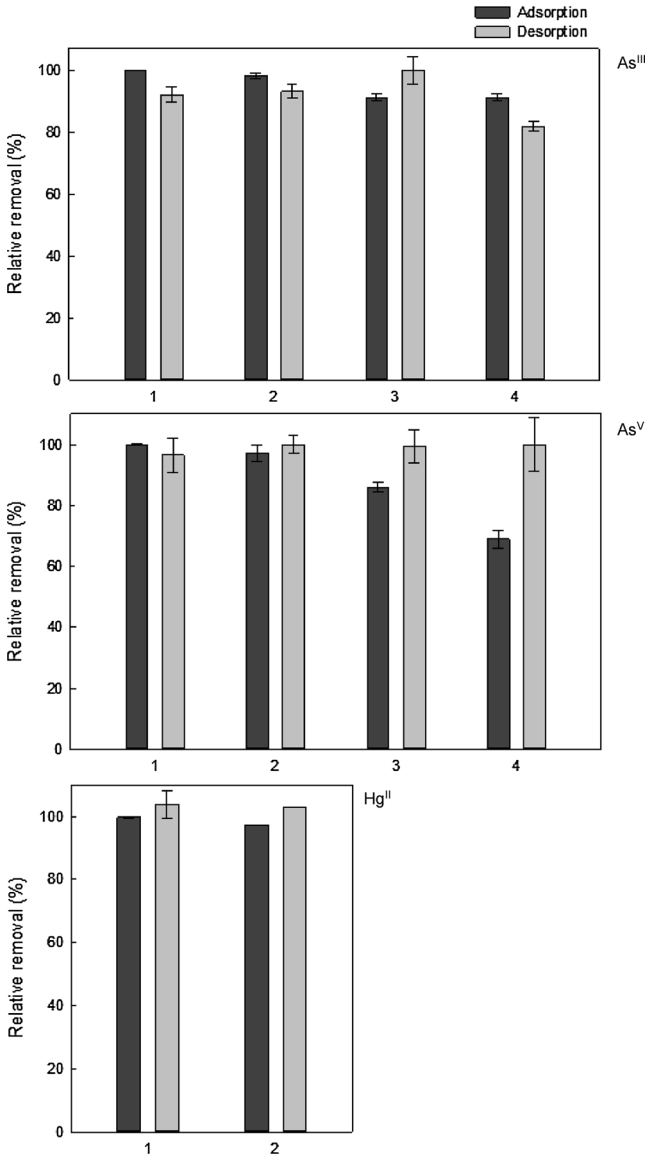

Fig. 8. Performance of γ-Fe_2O_3@CTF-1 during consecutive cycles of As^{III} (top), As^{V} (middle) and Hg^{II} (bottom) adsorption and desorption using 0.1 M NaOH for As and 0.1 M thiourea with 0.001 M HCl for Hg, both at 70 °C, illustrating the regenerability of the adsorbent. The error bars represent the standard deviation of $N = 3$ replicates.

for this investigation was partially funded by the Hercules foundation of the Flemish government. This work was supported by the Belgian IAP-PAI network.

Appendix A. Supplementary data

Supplementary material related to this article can be found, in the online version, at doi:https://doi.org/10.1016/j.jhazmat.2018.04.027.

References

[1] WHO, Arsenic in Drinking Water, W.H. Organisation, Geneva, Switzerland, 2011.
[2] European Commission, Council Directve 98/83/EC, in: Quality of water intented for human consumption, 2015.
[3] K. Folens, K. Leus, N.R. Nicomel, M. Meledina, S. Turner, G. Van Tendeloo, G.D. Laing, P. Van Der Voort, Fe3O4@MIL-101 – a selective and regenerable adsorbent for the removal of As species from water, Eur. J. Inorg. Chem. 27 (2016) 4395–4401.
[4] D. Mohan, C.U. Pittman, Arsenic removal from water/wastewater using adsorbents - a critical review, J. Hazard. Mater. 142 (2007) 1–53.
[5] M. Habuda-Stanic, M. Nujic, Arsenic removal by nanoparticles: a review, Environ. Sci. Pollut. R 22 (2015) 8094–8123.
[6] J.F. Liu, Z.S. Zhao, G.B. Jiang, Coating Fe3O4 magnetic nanoparticles with humic acid for high efficient removal of heavy metals in water, Environ. Sci. Technol. 42 (2008) 6949–6954.
[7] S. Tang, I. Lo, Magnetic nanoparticles: essential factors for sustainable environmental applications, Water Res. 47 (2013) 2613–2632.
[8] P. Dave, L. Chopda, Application of iron oxide nanomaterials for the removal of heavy metals, J. Nanotechnol. 246 (2014) 572–574.
[9] N.R. Nicomel, K. Leus, K. Folens, P. Van der Voort, G. Du Laing, Technologies for arsenic removal from water: current status and future perspectives, Int. J. Env Res. Pub He (2016) 13.
[10] S.Y. Ding, W. Wang, Covalent organic frameworks (COFs): from design to applications, Chem. Soc. Rev. 42 (2013) 548–568.
[11] P. Kuhn, M. Antonietti, A. Thomas, Porous, covalent triazine-based frameworks prepared by ionothermal synthesis, Angew. Chem. Int. Ed. 47 (2008) 3450–3453.
[12] K. Kamiya, R. Kamai, K. Hashimoto, S. Nakanishi, Platinum-modified covalent triazine frameworks hybridized with carbon nanoparticles as methanol-tolerant oxygen reduction electrocatalysts, Nat. Commun. (2014) 5.
[13] R. Gomes, P. Bhanja, A. Bhaumik, A triazine-based covalent organic polymer for efficient CO2 adsorption, Chem. Commun. 51 (2015) 10050–10053.
[14] L. Hao, J. Ning, B. Luo, B. Wang, Y.B. Zhang, Z.H. Tang, J.H. Yang, A. Thomas, L.J. Zhi, Structural evolution of 2D microporous covalent triazine-based framework toward the study of high-performance supercapacitors, J. Am. Chem. Soc. 137 (2015) 219–225.
[15] J.L. Liu, E.M. Zong, H.Y. Fu, S.R. Zheng, Z.Y. Xu, D.Q. Zhu, Adsorption of aromatic compounds on porous covalent triazine-based framework, J. Colloid Interf. Sci. 372 (2012) 99–107.
[16] A. Bhunia, S. Dey, M. Bous, C.Y. Zhang, W. von Rybinski, C. Janiak, High adsorptive properties of covalent triazine-based frameworks (CTFs) for surfactants from aqueous solution, Chem. Commun. 51 (2015) 484–486.
[17] M.P. Jian, B. Liu, G.S. Zhang, R.P. Liu, X.W. Zhang, Adsorptive removal of arsenic from aqueous solution by zeolitic imidazolate framework-8 (ZIF-8) nanoparticles, Colloid Surf. A 465 (2015) 67–76.
[18] T. Wang, K. Kailasam, P. Xiao, G.S. Chen, L.Q. Chen, L.H. Wang, J.L. Li, J.J. Zhu, Adsorption removal of organic dyes on covalent triazine framework (CTF), Micropor. Mesopor. Mater. 187 (2014) 63–70.
[19] W. Zhang, F. Liang, C. Li, L.-G. Qiu, Y.-P. Yuan, F.-M. Peng, X. Jiang, A.-J. Xie, Y.-H. Shen, J.-F. Zhu, Microwave-enhanced synthesis of magnetic porous covalent triazine-based framework composites for fast separation of organic dye from aqueous solution, J. Hazard. Mater. 186 (2011) 984–990.
[20] L. K. R. D., Recoil-Mössbauer spectral analysis software for Windows, University of Ottowa, in, 1998.
[21] T.P. Almeida, A.R. Muxworthy, T. Kasama, W. Williams, C. Damsgaard, C. Frandsen, T.J. Pennycook, R.E. Dunin-Borkowski, Effect of maghemization on the magnetic properties of nonstoichiometric pseudo-single-domain magnetite particles, Geochem. Geophys. Geosyst. 16 (2015) 2969–2979.
[22] S. Lin, D.N. Lu, Z. Liu, Removal of arsenic contaminants with magnetic gamma-Fe2O3 nanoparticles, Chem. Eng. J. 211 (2012) 46–52.
[23] M. Kilianova, R. Prucek, J. Filip, J. Kolarik, L. Kvitek, A. Panacek, J. Tucek, R. Zboril, Remarkable efficiency of ultrafine superparamagnetic iron(III) oxide nanoparticles toward arsenate removal from aqueous environment, Chemosphere 93 (2013) 2690–2697.
[24] M.C.S. Faria, R.S. Rosemberg, C.A. Bomfeti, D.S. Monteiro, F. Barbosa, L.C.A. Oliveira, M. Rodriguez, M.C. Pereira, J.L. Rodrigues, Arsenic removal from contaminated water by ultrafine delta-FeOOH adsorbents, Chem. Eng. J. 237 (2014) 47–54.
[25] P. Mondal, C.B. Majumder, B. Mohanty, Effects of adsorbent dose, its particle size and initial arsenic concentration on the removal of arsenic, iron and manganese from simulated ground water by Fe3+ impregnated activated carbon, J. Hazard. Mater. 150 (2008) 695–702.
[26] B.E. Reed, R. Vaughan, L.Q. Jiang, As(V.) As(III), Hg, and Pb removal by Fe-oxide impregnated activated carbon, J. Environ. Eng.-Asce 126 (2000) 869–873.
[27] S.J. Zhang, X.Y. Li, J.P. Chen, Preparation and evaluation of a magnetite-doped activated carbon fiber for enhanced arsenic removal, Carbon 48 (2010) 60–67.
[28] W.F. Chen, R. Parette, J.Y. Zou, F.S. Cannon, B.A. Dempsey, Arsenic removal by iron-modified activated carbon, Water Res. 41 (2007) 1851–1858.
[29] H.J. Zhu, Y.F. Jia, X. Wu, H. Wang, Removal of arsenic from water by supported nano zero-valent iron on activated carbon, J. Hazard. Mater. 172 (2009) 1591–1596.
[30] L. Lorenzen, J.S.J. Vandeventer, W.M. Landi, Factors affecting the mechanism of the adsorption of arsenic species on activated carbon, Min. Eng. 8 (1995) 557–569.
[31] A.K. Mishra, S. Ramaprabhu, Magnetite decorated multiwalled carbon nanotube based supercapacitor for arsenic removal and desalination of seawater, J. Phys. Chem. C 114 (2010) 2583–2590.
[32] Z. Velickovic, G.D. Vukovic, A.D. Marinkovic, M.S. Moldovan, A.A. Peric-Grujic, P.S. Uskokovic, M.D. Ristic, Adsorption of arsenate on iron(III) oxide coated ethylenediamine functionalized multiwall carbon nanotubes, Chem. Eng. J. 181 (2012) 174–181.
[33] E. Pehlivan, T.H. Tran, W.K.I. Ouédraogo, C. Schmidt, D. Zachmann, M. Bahadir, Removal of As(V) from aqueous solutions by iron coated rice husk, Fuel Process. Technol. 106 (2013) 511–517.
[34] C. Wang, H.J. Luo, Z.L. Zhang, Y. Wu, J. Zhang, S.W. Chen, Removal of As(III) and As(V) from aqueous solutions using nanoscale zero valent iron-reduced graphite oxide modified composites, J. Hazard. Mater. 268 (2014) 124–131.
[35] X. Hu, Z.H. Ding, A.R. Zimmerman, S.S. Wang, B. Gao, Batch and column sorption

of arsenic onto iron-impregnated biochar synthesized through hydrolysis, Water Res. 68 (2015) 206–216.
[36] A. Etale, B. Yalala, H. Tutu, D.C. Drake, Adsorptive removal of mercury from acid mine drainage: a comparison of silica and maghemite nanoparticles, Toxico. Enviro. Chem. 96 (2014) 542–554.
[37] S. Zhang, Y. Zhang, J. Liu, Q. Xu, H. Xiao, X. Wang, H. Xu, J. Zhou, Thiol modified Fe3O4@SiO2 as a robust, high effective, and recycling magnetic sorbent for mercury removal, Chem. Eng. J. 226 (2013) 30–38.
[38] J.-f. Liu, Z.-s. Zhao, G.-b. Jiang, Coating Fe3O4 magnetic nanoparticles with humic acid for High efficient removal of heavy metals in Water, Environ. Sci. Technol. 42 (2008) 6949–6954.
[39] X. Zhang, T. Wu, Y. Zhang, D.H.L. Ng, H. Zhao, G. Wang, Adsorption of Hg2+ by thiol functionalized hollow mesoporous silica microspheres with magnetic cores, RSC Adv. 5 (2015) 51446–51453.
[40] P.N. Diagboya, B.I. Olu-Owolabi, K.O. Adebowale, Synthesis of covalently bonded graphene oxide-iron magnetic nanoparticles and the kinetics of mercury removal, RSC Adv. 5 (2015) 2536–2542.
[41] L. Cui, X. Guo, Q. Wei, Y. Wang, L. Gao, L. Yan, T. Yan, B. Du, Removal of mercury and methylene blue from aqueous solution by xanthate functionalized magnetic graphene oxide: sorption kinetic and uptake mechanism, J. Colloid Interface Sci. 439 (2015) 112–120.
[42] L. Huang, M. He, B. Chen, B. Hu, A designable magnetic MOF composite and facile coordination-based post-synthetic strategy for the enhanced removal of Hg2+ from water, J. Mater. Chem. A 3 (2015) 11587–11595.
[43] L. Huang, M. He, B. Chen, B. Hu, A mercapto functionalized magnetic Zr-MOF by solvent-assisted ligand exchange for Hg2++ removal from water, J. Mater. Chem. A 4 (2016) 5159–5166.
[44] D.E. Giles, M. Mohapatra, T.B. Issa, S. Anand, P. Singh, Iron and aluminium based adsorption strategies for removing arsenic from water, J. Environ. Manage 92 (2011) 3011–3022.
[45] R. Singh, S. Singh, P. Parihar, V.P. Singh, S.M. Prasad, Arsenic contamination, consequences and remediation techniques: a review, Ecotoxicol. Environ. Safe 112 (2015) 247–270.
[46] W.S. Tang, Q. Li, S.A. Gao, J.K. Shang, Arsenic (III,V) removal from aqueous solution by ultrafine alpha-Fe2O3 nanoparticles synthesized from solvent thermal method, J. Hazard. Mater. 192 (2011) 131–138.
[47] D. Maity, D.C. Agrawal, Synthesis of iron oxide nanoparticles under oxidizing environment and their stabilization in aqueous and non-aqueous media, J. Magn. Magn. Mater. 308 (2007) 46–55.
[48] A.-H. Lu, E.L. Salabas, F. Schüth, Magnetic manoparticles: synthesis, protection, functionalization, and application, Angew. Chem. Int. Ed. 46 (2007) 1222–1244.
[49] P. Sharma, A. Kappler, Desorption of arsenic from clay and humic acid-coated clay by dissolved phosphate and silicate, J. Contam. Hydrol. 126 (2011) 216–225.
[50] P. Sharma, A. Kappler, Desorption of arsenic from clay and humic acid-coated clay by dissolved phosphate and silicate, J. Contam. Hydrol. 126 (2011) 216–225.